Improved time-frequency representation for non-stationary vibrations of slow rotating machinery

Cédric Peeters[1], Andreas Jakobsson [2], Jérôme Antoni[3], and Jan Helsen[1]

[1] *Department of Applied Mechanics, Vrije Universiteit Brussel, Brussels, Belgium*
cedric.peeters@vub.be
jan.helsen@vub.be

[2] *Center for Mathematical Sciences, Lund University, Sweden*
andreas.jakobsson@matstat.lu.se

[3] *Univ Lyon, INSA Lyon, LVA, Villeurbanne, France*
jerome.antoni@insa-lyon.fr

ABSTRACT

The short-time Fourier transform (STFT) is a staple analysis tool for vibration signal processing due to it being a robust, non-parametric, and computationally efficient technique to analyze non-stationary signals. However, despite these beneficial properties, the STFT suffers from high variance, high sidelobes, and a low resolution. This paper investigates an alternative non-parametric method, namely the sliding-window iterative adaptive approach, to use for time-frequency representations of non-stationary vibrations. This method reduces the sidelobe levels and allows for high resolution estimates. The performance of the method is evaluated on both simulated and experimental vibration data of slow rotating machinery such as a multi-megawatt wind turbine gearbox. The results indicate significant benefits as compared to the STFT with regard to accuracy, readability, and versatility.

1. INTRODUCTION

Spectral analysis of vibration signals plays a crucial role in the majority of existing condition monitoring schemes. A commonly employed spectral analysis tool to investigate vibrations from machinery operating in non-stationary conditions is the visualisation of time-frequency representations (TFRs). These TFRs of vibration signals can be valuable for various reasons and have therefore been used for multiple different purposes. Example usages in vibration analysis include tracking the amplitudes of specific signal components over time (Sapena-Bano, Burriel-Valencia, Pineda-Sanchez, Puche-Panadero, & Riera-Guasp, 2016), assessing the degree of non-stationarity (Martin & Mailhes, 2009), extracting rotating speed information (Peeters et al., 2019), separating asynchronous harmonics (Chen & Feng, 2021), and whitening the signal (Leclere, André, & Antoni, 2016). Research into improving existing TFR techniques has been ongoing and plentiful for the last few decades with many new techniques for TF decompositions having been developed, e.g. (Shensa et al., 1992; Barkat & Boashash, 1999; Greitans, 2005; Gardner & Magnasco, 2006; Wang, 2007; Wang & Orchard, 2009; Du, Li, Stoica, Ling, & Ram, 2009; Zhang & Castagna, 2011; Daubechies, Lu, & Wu, 2011; Oberlin, Meignen, & Perrier, 2014). While TFRs can be a precursor to other post-processing methods such as rotating speed estimation techniques, they can also serve as direct tools for fault detection. An example of such a use-case is the tracking of non-stationary transient signatures in a TFR over different frequency bands for bearing fault detection (Wang et al., 2019).

The analysis of multicomponent signals through TFRs is a much researched topic in the signal processing literature. One reason why there is so much literature about time-frequency (TF) analysis is the wide range of application domains, e.g. acoustics (Neal, Briggs, Raich, & Fern, 2011; Baydar & Ball, 2001), structural and machine health monitoring (Baydar & Ball, 2001; Feng, Liang, & Chu, 2013; He, 2013; Peng, Li, Hao, & Xin, 2020), physiological signals (Bozkurt, Germanakis, & Stylianou, 2018), astronomy (Liu, Zhang, & Shan, 2018), hydrology (Labat, 2005), seismology (Spanos, Giaralis, & Politis, 2007), climatology (Torrence & Compo, 1998; Salisbury & Wimbush, 2002; Kravchinsky, Langereis, Walker, Dlusskiy, & White, 2013), ecology (Cazelles et al., 2008), and geology (Reager, Thomas, & Famiglietti, 2014). Some common non-parametric TF techniques include

the STFT (Flanagan & Golden, 1966), Wigner-Ville Distribution (WVD) (Wigner, 1932), Choi-Williams Distribution (CWD) (Choi & Williams, 1989), S-transform (Stockwell, Mansinha, & Lowe, 1996), and the chirplet transform (Mann & Haykin, 1991). These methods have all been used in the past for vibration analysis and monitoring as they form an appealing choice thanks to being hyperparameter-free. However, making no signal model assumptions can also be disadvantageous and most of these techniques are considered to have drawbacks depending on the intended application. This can be illustrated with the STFT, which uses a constant window size for both low and high frequencies, introducing a trade-off between time and frequency resolution. The efficacy of the STFT is thus hindered by the window choice as the Heisenberg uncertainty principle (Gabor, 1946) limits the achievable adaptability of the STFT. Similarly, the original definition of the WVD has an obvious downside thanks to the presence of large cross-terms between every pair of signal components and between positive and negative frequencies. The CWD suppresses the cross-terms of the WVD, but still suffers from aliasing for transients where a frequency component can be replicated at a distance π (Zheng & McFadden, 1999). While the S-transform is similar to the wavelet transform in that it offers a higher time resolution with lower frequency resolution at high frequencies and a higher frequency resolution with lower time resolution at low frequencies, it therefore also suffers from the same drawback that this resolution trade-off might not be desirable.

Despite the existence of this variety of TFR methods, probably the short-time Fourier transform (STFT) remains the most used conventional technique due to it being an easy-to-interpret non-parametric TFR method with low computational complexity and no model assumptions. The STFT is also reliable for the analysis of complex vibrations that contain an unknown number of non-stationary signal components with varying or low signal-to-noise ratios (SNR), a property which is not always shared by some other, typically parametric, developments that need a prior estimate of the number of signal components. For integration into an automated vibration processing methodology, the benefit of having a standalone method that does not require any data-dependent hyperparameter setting is quite a significant one. When large amounts of highly variable vibration data need to be processed, it is simply not feasible to optimize these hyperparameters for each dataset.

This paper investigates the potential of an adaptive spectral estimation alternative to the STFT method for vibration analysis that offers a reduction in leakage effects in exchange for a higher computational complexity. The sliding-window or short-time iterative adaptive approach (ST-IAA) is a high-resolution data-dependent filterbank-based approach that has been briefly investigated in the past for passive sensing and radar applications (Du et al., 2009) and also for human gait analysis (Du et al., 2009). However, these applications involve vastly different signal complexities when compared to vibrations measured on complex machinery. This work therefore analyses the performance of the ST-IAA on such complex vibration signals with a focus on slow rotating machinery and it tries to lay the groundwork for more advanced applications in vibration analysis of the ST-IAA and similar techniques in the future. Section 2 introduces the theory behind the short-time iterative adaptive approach, whilst sections 3 and 4 illustrate the technique on realistic simulated vibration signals and experimental data, respectively. The results and next steps are discussed in section 5.

2. METHODOLOGY

The Iterative Adaptive Approach (IAA) is a spectral estimation technique that gained a lot of interest in the early years of the previous decade for the purpose of source localization, pulse compression, and missing data estimation (Yardibi, Li, Stoica, Xue, & Baggeroer, 2010; Karlsson, Rowe, Xu, Glentis, & Li, 2014). It is an iterative weighted least-squares method that is non-parametric and thus easy to use. It has been shown in the past that the IAA can reduce sidelobe levels and yield a higher resolution than the standard periodogram. Additionally, it also returns a dense (i.e., not sparse) estimate of the signal power spectrum which can be beneficial when dealing with complex vibrations, since enforcing sparsity typically involves parameter tuning. IAA assumes that the vibration data adheres to the following signal model:

$$\boldsymbol{y}_N = \boldsymbol{F}_{N,K}\boldsymbol{\alpha}_K + \boldsymbol{e}_N \tag{1}$$

with $\boldsymbol{y}_N \in \mathbb{R}^{\mathrm{N}}$ being the vibration signal of length N, $\boldsymbol{F}_{N,K} \triangleq [\boldsymbol{f}_N(\omega_0), \boldsymbol{f}_N(\omega_1), ..., \boldsymbol{f}_N(\omega_{K-1})]$ the Fourier matrix of size $(N\mathrm{x}K)$, $\boldsymbol{\alpha}_K \triangleq [\alpha(\omega_0), \alpha(\omega_1), ..., \alpha(\omega_{K-1})]^T$ the complex-valued spectral amplitudes at the frequencies ω_k, and $\boldsymbol{e}_N$ an additive noise. IAA tries to estimate $\boldsymbol{\alpha}_K$ from Eq. 1 by minimizing the following weighted least-squares cost function:

$$||\boldsymbol{y}_N - \boldsymbol{f}_N(\omega_k)\alpha_k||^2_{\boldsymbol{Q}_N^{-1}(\omega_k)}, k = 0, 1, ..., K-1 \tag{2}$$

where $||\boldsymbol{z}||^2_{\boldsymbol{Q}_N^{-1}(\omega_k)} \triangleq \boldsymbol{z}^H\boldsymbol{Q}_N^{-1}(\omega_k)\boldsymbol{z}$ and:

$$\boldsymbol{Q}_N(\omega_k) = \boldsymbol{R}_N - p_k\boldsymbol{f}_N(\omega_k)\boldsymbol{f}_N^H(\omega_k) \tag{3}$$

is the noise and IAA interference (signals at frequency grid points bar ω_k) covariance matrix for the kth grid point. The signal power is denoted by $p_k = |\alpha_k|^2$ and the IAA covariance matrix is given by:

$$\boldsymbol{R}_N = \boldsymbol{F}_{N,K}\boldsymbol{P}_K\boldsymbol{F}_{N,K}^H \tag{4}$$

with $\boldsymbol{P}_K$ a diagonal matrix with p_k on its main diagonal. Minimisation of Eq. 2 for α_k (with p_k kept constant) $k =$

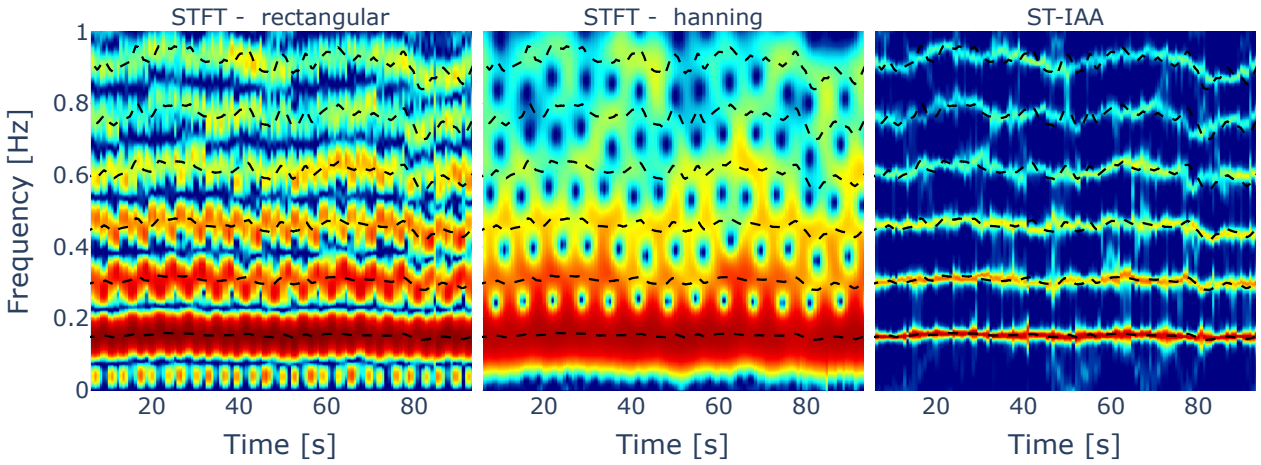

Figure 1. (Left) TFR using the STFT with a rectangular window, (Center) TFR using the STFT with a Hanning window, (Right) TFR using the ST-IAA. The black dashed lines represent the true input frequency of the simulated harmonics.

$0, 1, ..., K-1$ results in (see Appendix A for the derivation):

$$\alpha_k^{IAA} = \frac{\boldsymbol{f}_N^H(\omega_k)\boldsymbol{Q}_N^{-1}(\omega_k)\boldsymbol{y}_N}{\boldsymbol{f}_N^H(\omega_k)\boldsymbol{Q}_N^{-1}(\omega_k)\boldsymbol{f}_N(\omega_k)},\ k = 0, 1, ..., K-1. \tag{5}$$

This can be simplified using Eq. 3 and the matrix inversion lemma (Horn & Johnson, 1985; Yardibi et al., 2010) to:

$$\alpha_k^{IAA} = \frac{\boldsymbol{f}_N^H(\omega_k)\boldsymbol{R}_N^{-1}\boldsymbol{y}_N}{\boldsymbol{f}_N^H(\omega_k)\boldsymbol{R}_N^{-1}\boldsymbol{f}_N(\omega_k)},\ k = 0, 1, ..., K-1. \tag{6}$$

Equation 6 reduces the computational cost drastically since it does not necessitate the computation of $\boldsymbol{Q}_N^{-1}(\omega_k)$ for each frequency bin k.

Since the signal power P_K is required in Eq. 6, the IAA estimate needs to be computed iteratively. In this paper, the periodogram is used to initialize the IAA estimate. To speed up computations, the fast implementation of the IAA using the Gohberg-Semencul representations and trigonometric polynomials is employed, for more details see (Glentis & Jakobsson, 2011).

To get the short-time IAA (ST-IAA) time-frequency representation of the vibration signal, a sliding window approach is used similar to the STFT. In case minimal computation time is crucial, further optimizations can be made by approximating the ST-IAA, e.g. by assuming the covariance matrix does not change drastically from one window to the next (i.e. for window i $\boldsymbol{R}_N^i \approx \boldsymbol{R}_N^{i-1}$), or by incorporating a single step steepest descent scheme instead of using the Levinson-Durbin algorithm in the efficient formulation of the IAA (for more details, see (Glentis & Jakobsson, 2010)). In this paper, the standard ST-IAA is used without the two mentioned optimizations.

3. Simulation Results

To analyse the performance of the ST-IAA and compare it with the STFT, a non-stationary vibration signal is simulated that is representative of a slow rotating machine. The vibration $x(n)$ with a sample period of T consists of multiple harmonics with additive white Gaussian noise ν and is described by following signal model:

$$x(n) = \sum_{m=1}^{M} A_m sin(2\pi T \sum_{n=0}^{N-1} f_m(n)) + \nu(n) \tag{7}$$

where $m = 1, 2, ..., M$ is the harmonic number, A_m is the amplitude of harmonic m, $n = 0, 1, ..., N-1$ is the sample number, and $f_m(n)$ is the varying frequency vector of harmonic m.

The simulated signal is 100 seconds long and consists of 6 harmonics of a fundamental frequency at 0.15 Hz that varies randomly but smoothly around this base frequency. The amplitudes decrease inversely with the harmonic number. The same input parameters are used for the STFT as for the ST-IAA, viz. a window length of 200 samples, an overlap of 95%, and a grid size of 8000 samples. Figure 1 shows the TFRs for the STFT using both a rectangular and hanning window next to the TFR using the ST-IAA.

As can be seen from Fig. 1, the ST-IAA produces a far clearer TFR to interpret due to the much narrower peaks and reduced sidelobe levels. The normalized Renyi entropy, which has often been employed in the past when measuring TFR complexity (Flandrin, Baraniuk, & Michel, 1994; Baraniuk, Flandrin, Janssen, & Michel, 2001; Sucic, Saulig, & Boashash, 2011;

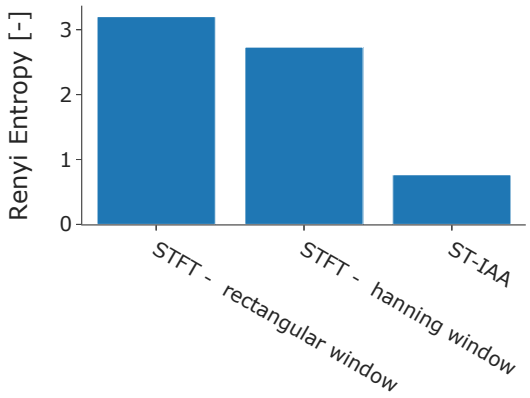

Figure 2. Renyi entropies for the three investigated TFRs shown in Fig. 1 with $\alpha = 3$.

Colominas, Jomaa, Jrad, Humeau-Heurtier, & Van Bogaert, 2017), is used to compare the complexity of each TFR. The normalized Renyi entropy of order α for a discrete-time TFR $P_x(n,k)$ is defined as follows:

$$R_\alpha = \frac{1}{1-\alpha} log_2\Big(\frac{\sum_{n=0}^{N}\sum_{k=0}^{K} P_x^\alpha(n,k)}{\sum_{n=0}^{N}\sum_{k=0}^{K} P_x(n,k)}\Big) \qquad (8)$$

where n is the discrete time variable and k the frequency bin. The third-order ($\alpha = 3$) Renyi entropy is chosen for the comparison as it was found to be most suitable for the intended purpose of TFR complexity quantification (Williams, Brown, & Hero III, 1991; Flandrin et al., 1994; Williams, 1996; Baraniuk et al., 2001). The Renyi entropies for the three TFRs of Fig. 1 are shown in Fig. 2. The ST-IAA exhibits a considerably lower Renyi entropy when compared to the STFT. While Renyi entropy is not a perfect measure to quantify the accuracy and robustness of a TFR, it does corroborate the visual interpretation of Fig. 1.

To further illustrate the improved resolution of the ST-IAA as compared to the STFT, a simple maximum tracking is done over time for the different harmonics. This is a straightforward approach to estimate rotation speeds of a machine without needing much processing power or signal processing know-how and is thus often utilized in industry. Figure 3 shows the estimated curves for each of the harmonics using the same input parameters for all three TFRs of Fig. 1. As can be seen visually, the tracking error is considerably lower for the ST-IAA as compared to the STFT. This observation is quantified by the mean square error as displayed in Fig. 4.

4. Experimental results

To evaluate the utility of the short-time IAA in real-world scenarios, it is compared to the STFT with a rectangular window on a vibration data set measured on the drivetrain of an offshore multi-megawatt wind turbine. Accelerometers were installed spread out over the drivetrain together with a single-pulse-per-revolution angle encoder on the high-speed shaft of the gearbox. All measurements were acquired at a sample rate of 20kHz for a duration of 10 seconds. The speed estimation from the angle encoder provides a means to assess the accuracy of the ST-IAA for tracking the speed-dependent harmonics generated by the mechanical components on top of the visual improvement in the time-frequency representations that enhance its interpretability.

Figure 5 displays the TFRs of the STFT and ST-IAA for a vibration signal measured on the first planetary gearbox stage. The used input parameters are identical for both TFRs. A window of 4 seconds is used with an overlap of 99%. Each windowed signal is also zero-padded till 40 seconds, i.e., a zero-padding factor of 10. The TFRs are zoomed in on the low frequency range from 0 to 1 Hz. Typically, the 3P frequency (i.e., three times the rotor speed) forms a distinct signature in this sub-1Hz-region for a three-bladed rotor. This is exactly what is visible in Fig. 5 around 0.68 Hz. There is another lower frequency harmonic present but this is an interfering non-speed related harmonic from a adjacent component, that also coincides partly with the first side-side natural frequency of the tower. Unfortunately the measurement duration of 10 seconds is too short to clearly distinguish between these two components.

To quantify this perceived accuracy of the ST-IAA in Fig 5 for post-processing techniques such as maximum tracking, the mean and median absolute errors are shown for both the STFT and ST-IAA in Fig. 6. As can be observed from Fig. 6, the errors are lower for ST-IAA as compared to the STFT, indicating that the ST-IAA is also at least as reliable as the STFT with regard to accuracy even for experimental vibration signals.

To further illustrate the potential of the ST-IAA for the analysis of noisy vibration signals, Figure 7 shows the STFT and ST-IAA TFRs for the high-speed stage sensor zoomed around the rotational speed of the high-speed shaft. The encoder speed is shown by a black full line and coincides with the high-speed shaft harmonic. However, while the high-speed shaft harmonic around 24 Hz can be observed, its SNR is considerably lower than the gear meshing frequency of the first planetary stage around 23 Hz. It is also easier to distinguish in the ST-IAA than the STFT. The same exercise in maximum tracking is done for the high-speed shaft harmonic. The estimated curve is shown in Fig. 7 by the dashed black line. The mean and median absolute errors are displayed in Fig. 8, which corroborates again the efficacy of the ST-IAA

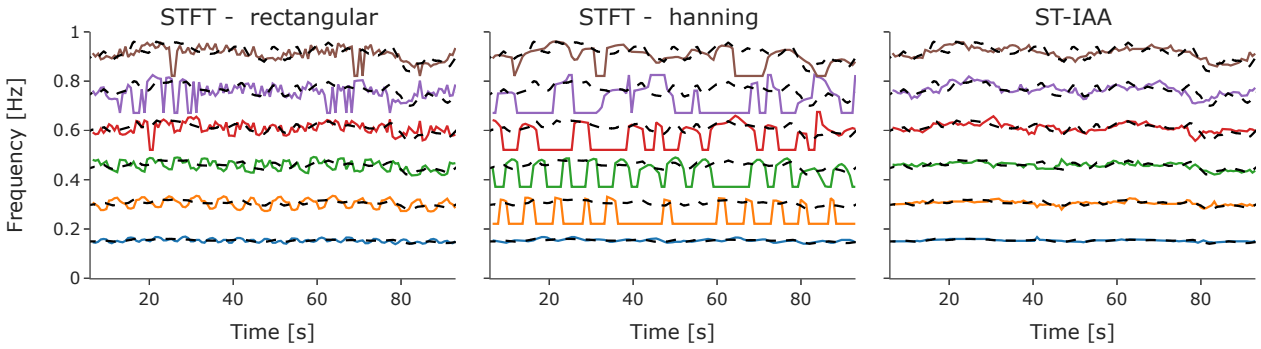

Figure 3. Estimated harmonic frequencies based on maximum tracking in a band around each harmonic for the three investigated TFRs shown in Fig. 1.

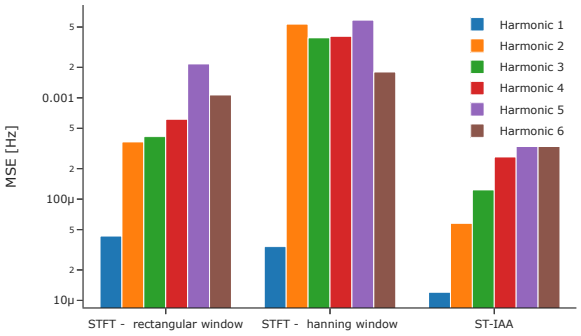

Figure 4. Mean square error of the estimated harmonic frequencies based on maximum tracking in the TFRs of Fig. 1.

in improving the STFT at the cost of additional computation time.

5. Conclusion

This paper investigates the potential of the short-time iterative adaptive approach (ST-IAA) as a robust and accurate non-parametric spectral estimator for time-frequency representations (TFRs). It evaluates and compares the ST-IAA to the short-time Fourier transform (STFT) on both simulated and experimental wind turbine vibration data. The ST-IAA shows that it suffers significantly less from high sidelobe levels which the STFT does suffer from and reduces both the interpretability of the time-frequency representation and its potential for post-processing techniques. For example, techniques that employ the TFR for tracking harmonic frequencies can be hindered by such high sidelobe levels as is shown in both the simulation and experimental investigation. The main downside of the ST-IAA is its computation time which is considerably higher than that of the STFT. However, fast implementations of the ST-IAA do exist that alleviate some of this computational burden.

Acknowledgment

Cédric Peeters and Jan Helsen received funding from the Flemish Government (AI Research Program). They would like to acknowledge FWO (FondsWetenschappelijk Onderzoek) for their support through the postdoctoral grant of Cédric Peeters (1282221N). They would also like to acknowledge FWO for the support through the SBO Robustify project (S006119N).

Appendix A

Minimizing the weighted least-squares cost function in Eq. 2 boils down to finding α_k for which the derivative of the cost function with respect to α_k or its conjugate is zero. To simplify the notation, the dependency of f_N and $\boldsymbol{Q}_N^{-1}$ on ω_k is dropped. The derivative can then be expressed and simplified as follows:

$$\frac{\delta}{\delta \alpha_k^H}\left[(\boldsymbol{y}_N - \boldsymbol{f}_N\alpha_k)^H \boldsymbol{Q}_N^{-1}(\boldsymbol{y}_N - \boldsymbol{f}_N\alpha_k)\right] = 0 \tag{9}$$

$$\frac{\delta}{\delta \alpha_k^H}\Big[\boldsymbol{y}_N^H\boldsymbol{Q}_N^{-1}\boldsymbol{y}_N - \alpha_k^H\boldsymbol{f}_N^H\boldsymbol{Q}_N^{-1}\boldsymbol{y}_N - \alpha_k\boldsymbol{y}_N^H\boldsymbol{Q}_N^{-1}\boldsymbol{f}_N + \alpha_k^H\alpha_k\boldsymbol{f}_N^H\boldsymbol{Q}_N^{-1}\boldsymbol{f}_N\Big] = 0 \tag{10}$$

$$-\boldsymbol{f}_N^H\boldsymbol{Q}_N^{-1}\boldsymbol{y}_N + \alpha_k\boldsymbol{f}_N^H\boldsymbol{Q}_N^{-1}\boldsymbol{f}_N = 0 \tag{11}$$

$$\alpha_k^{IAA} = \frac{\boldsymbol{f}_N^H\boldsymbol{Q}_N^{-1}\boldsymbol{y}_N}{\boldsymbol{f}_N^H\boldsymbol{Q}_N^{-1}\boldsymbol{f}_N} \tag{12}$$

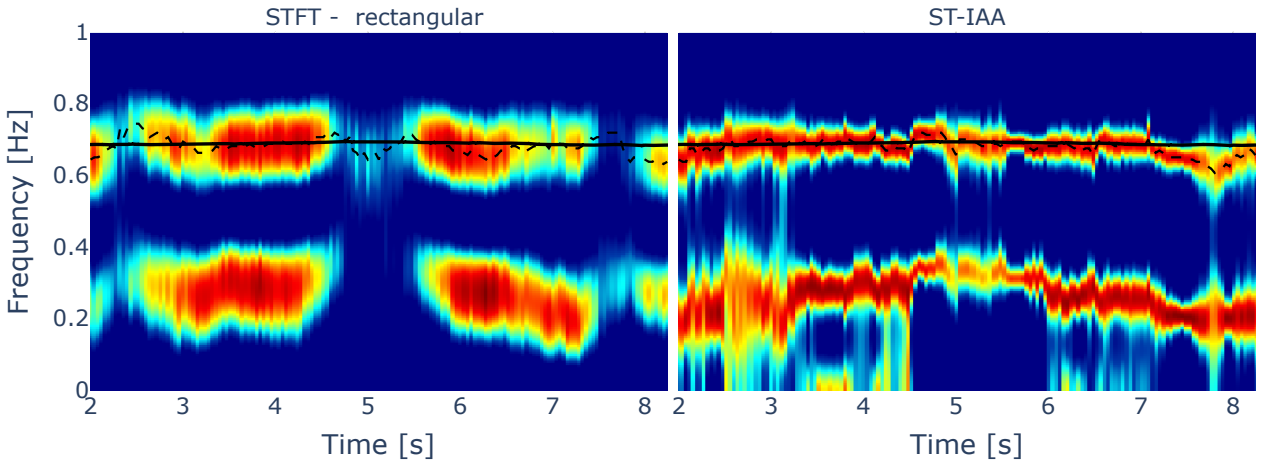

Figure 5. (Left) TFR of the vibration measured by the accelerometer installed on the first planetary gearbox stage using the STFT with a rectangular window, (Right) TFR of the same vibration but using the ST-IAA. The black full line represents the speed measured by the angle encoder while the dashed lines represent the estimated harmonic frequency based on maximum tracking.

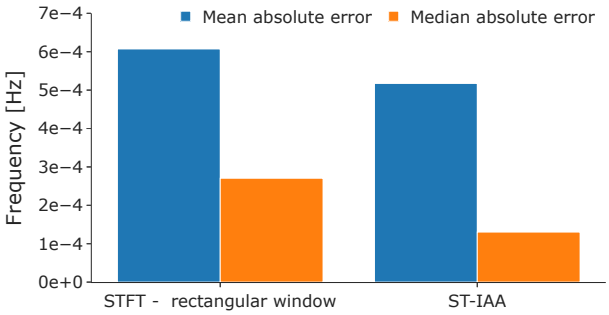

Figure 6. Mean and median absolute error between the estimated 3P harmonic frequency using maximum tracking and the encoder-based speed for the STFT (left) and the ST-IAA (right).

It can be seen that Eq. 12 is thus the same as the one in Eq. 2 for a single grid point k.

References

Baraniuk, R. G., Flandrin, P., Janssen, A. J., & Michel, O. J. (2001). Measuring time-frequency information content using the rényi entropies. *IEEE Transactions on Information theory*, *47*(4), 1391–1409.

Barkat, B., & Boashash, B. (1999). Design of higher order polynomial wigner-ville distributions. *IEEE Transactions on Signal Processing*, *47*(9), 2608–2611.

Baydar, N., & Ball, A. (2001). A comparative study of acoustic and vibration signals in detection of gear failures using wigner–ville distribution. *Mechanical systems and signal processing*, *15*(6), 1091–1107.

Bozkurt, B., Germanakis, I., & Stylianou, Y. (2018). A study of time-frequency features for cnn-based automatic heart sound classification for pathology detection. *Computers in biology and medicine*, *100*, 132–143.

Cazelles, B., Chavez, M., Berteaux, D., Ménard, F., Vik, J. O., Jenouvrier, S., & Stenseth, N. C. (2008). Wavelet analysis of ecological time series. *Oecologia*, *156*(2), 287–304.

Chen, X., & Feng, Z. (2021). Order spectrum analysis enhanced by surrogate test and vold-kalman filtering for rotating machinery fault diagnosis under time-varying speed conditions. *Mechanical Systems and Signal Processing*, *154*, 107585.

Choi, H.-I., & Williams, W. J. (1989). Improved time-frequency representation of multicomponent signals using exponential kernels. *IEEE Transactions on Acoustics, Speech, and Signal Processing*, *37*(6), 862–871.

Colominas, M. A., Jomaa, M. E. S. H., Jrad, N., Humeau-Heurtier, A., & Van Bogaert, P. (2017). Time-varying time–frequency complexity measures for epileptic eeg data analysis. *IEEE transactions on biomedical engineering*, *65*(8), 1681–1688.

Daubechies, I., Lu, J., & Wu, H.-T. (2011). Syn-

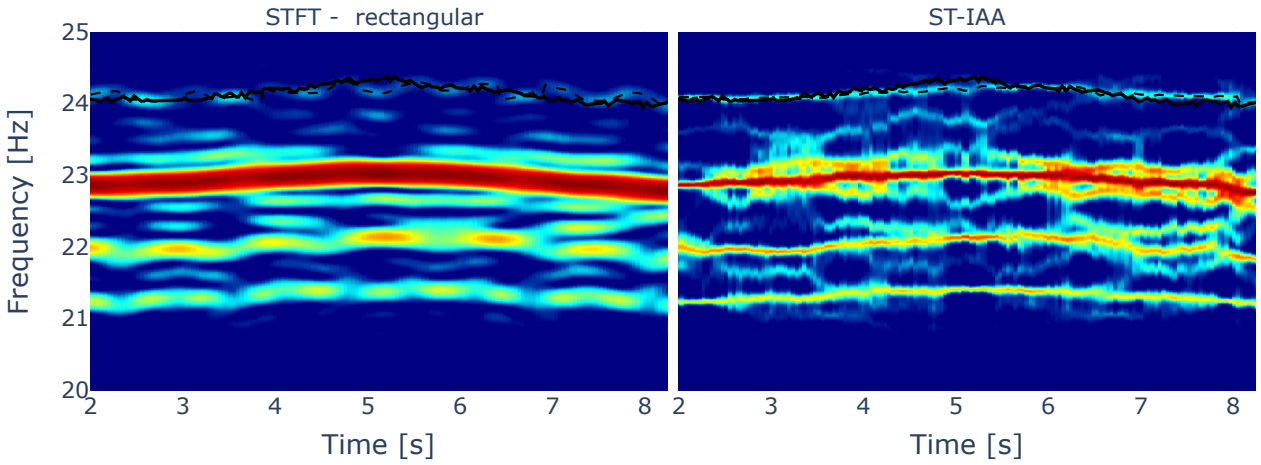

Figure 7. (Left) TFR of the vibration measured by the accelerometer installed on the high-speed gear stage using the STFT with a rectangular window, (Right) TFR of the same vibration but using the ST-IAA. The black full line represents the speed measured by the angle encoder while the dashed lines represent the estimated harmonic frequency based on maximum tracking.

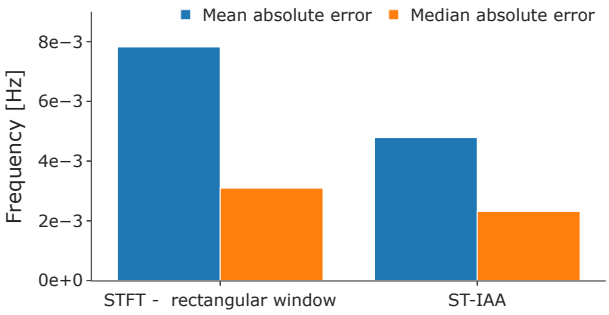

Figure 8. Mean and median absolute error between the estimated high-speed shaft harmonic frequency using maximum tracking and the encoder-based speed for the STFT (left) and the ST-IAA (right).

chrosqueezed wavelet transforms: An empirical mode decomposition-like tool. *Applied and computational harmonic analysis*, *30*(2), 243–261.

Du, L., Li, J., Stoica, P., Ling, H., & Ram, S. S. (2009). Doppler spectrogram analysis of human gait via iterative adaptive approach. *Electronics letters*, *45*(3), 186–188.

Feng, Z., Liang, M., & Chu, F. (2013). Recent advances in time–frequency analysis methods for machinery fault diagnosis: A review with application examples. *Mechanical Systems and Signal Processing*, *38*(1), 165–205.

Flanagan, J. L., & Golden, R. (1966). Phase vocoder. *Bell System Technical Journal*, *45*(9), 1493–1509.

Flandrin, P., Baraniuk, R. G., & Michel, O. (1994). Time-frequency complexity and information. In *Proceedings of icassp'94. ieee international conference on acoustics, speech and signal processing* (Vol. 3, pp. III–329).

Gabor, D. (1946). Theory of communication. part 1: The analysis of information. *Journal of the Institution of Electrical Engineers-Part III: Radio and Communication Engineering*, *93*(26), 429–441.

Gardner, T. J., & Magnasco, M. O. (2006). Sparse time-frequency representations. *Proceedings of the National Academy of Sciences*, *103*(16), 6094–6099.

Glentis, G.-O., & Jakobsson, A. (2010). Time-recursive iaa spectral estimation. *IEEE Signal Processing Letters*, *18*(2), 111–114.

Glentis, G.-O., & Jakobsson, A. (2011). Efficient implementation of iterative adaptive approach spectral estimation techniques. *IEEE Transactions on Signal Processing*, *59*(9), 4154–4167.

Greitans, M. (2005). Adaptive stft-like time-frequency analysis from arbitrary distributed signal samples. In *International workshop on sampling theory and application, samsun, turkey.*

He, Q. (2013). Time–frequency manifold for nonlinear feature extraction in machinery fault diagnosis. *Mechanical Systems and Signal Processing*, *35*(1-2), 200–218.

Horn, R., & Johnson, C. (1985). Matrix analysis, cambridge univ. *Press. MR0832183*.

Karlsson, J., Rowe, W., Xu, L., Glentis, G.-O., & Li, J. (2014). Fast missing-data iaa with application to

notched spectrum sar. *IEEE Transactions on Aerospace and Electronic Systems*, *50*(2), 959–971.

Kravchinsky, V. A., Langereis, C. G., Walker, S. D., Dlusskiy, K. G., & White, D. (2013). Discovery of holocene millennial climate cycles in the asian continental interior: Has the sun been governing the continental climate? *Global and planetary change*, *110*, 386–396.

Labat, D. (2005). Recent advances in wavelet analyses: Part 1. a review of concepts. *Journal of Hydrology*, *314*(1-4), 275–288.

Leclere, Q., André, H., & Antoni, J. (2016). A multi-order probabilistic approach for instantaneous angular speed tracking debriefing of the cmmno 14 diagnosis contest. *Mechanical Systems and Signal Processing*, *81*, 375–386.

Liu, S., Zhang, Y. D., & Shan, T. (2018). Detection of weak astronomical signals with frequency-hopping interference suppression. *Digital Signal Processing*, *72*, 1–8.

Mann, S., & Haykin, S. (1991). The chirplet transform: A generalization of gabor's logon transform. In *Vision interface* (Vol. 91, pp. 205–212).

Martin, N., & Mailhes, C. (2009). A non-stationary index resulting from time and frequency domains. In *Sixth international conference on condition monitoring and machinery failure prevention technologies. cm 2009 and mfpt 2009.*

Neal, L., Briggs, F., Raich, R., & Fern, X. Z. (2011). Time-frequency segmentation of bird song in noisy acoustic environments. In *2011 ieee international conference on acoustics, speech and signal processing (icassp)* (pp. 2012–2015).

Oberlin, T., Meignen, S., & Perrier, V. (2014). The fourier-based synchrosqueezing transform. In *2014 ieee international conference on acoustics, speech and signal processing (icassp)* (pp. 315–319).

Peeters, C., Leclere, Q., Antoni, J., Lindahl, P., Donnal, J., Leeb, S., & Helsen, J. (2019). Review and comparison of tacholess instantaneous speed estimation methods on experimental vibration data. *Mechanical Systems and Signal Processing*, *129*, 407–436.

Peng, Z., Li, J., Hao, H., & Xin, Y. (2020). High-resolution time-frequency representation for instantaneous frequency identification by adaptive duffing oscillator. *Structural Control and Health Monitoring*, *27*(12), e2635.

Reager, J., Thomas, B., & Famiglietti, J. (2014). River basin flood potential inferred using grace gravity observations at several months lead time. *Nature Geoscience*, *7*(8), 588–592.

Salisbury, J., & Wimbush, M. (2002). Using modern time series analysis techniques to predict enso events from the soi time series. *Nonlinear Processes in Geophysics*, *9*(3/4), 341–345.

Sapena-Bano, A., Burriel-Valencia, J., Pineda-Sanchez, M., Puche-Panadero, R., & Riera-Guasp, M. (2016). The harmonic order tracking analysis method for the fault diagnosis in induction motors under time-varying conditions. *IEEE Transactions on Energy Conversion*, *32*(1), 244–256.

Shensa, M. J., et al. (1992). The discrete wavelet transform: wedding the a trous and mallat algorithms. *IEEE Transactions on signal processing*, *40*(10), 2464–2482.

Spanos, P., Giaralis, A., & Politis, N. (2007). Time–frequency representation of earthquake accelerograms and inelastic structural response records using the adaptive chirplet decomposition and empirical mode decomposition. *Soil Dynamics and Earthquake Engineering*, *27*(7), 675–689.

Stockwell, R. G., Mansinha, L., & Lowe, R. (1996). Localization of the complex spectrum: the s transform. *IEEE transactions on signal processing*, *44*(4), 998–1001.

Sucic, V., Saulig, N., & Boashash, B. (2011). Estimating the number of components of a multicomponent nonstationary signal using the short-term time-frequency rényi entropy. *EURASIP Journal on Advances in Signal Processing*, *2011*(1), 1–11.

Torrence, C., & Compo, G. P. (1998). A practical guide to wavelet analysis. *Bulletin of the American Meteorological society*, *79*(1), 61–78.

Wang, Y. (2007). Seismic time-frequency spectral decomposition by matching pursuit. *Geophysics*, *72*(1), V13–V20.

Wang, Y., & Orchard, J. (2009). Fast discrete orthonormal stockwell transform. *SIAM Journal on Scientific Computing*, *31*(5), 4000–4012.

Wang, Y., Peter, W. T., Tang, B., Qin, Y., Deng, L., Huang, T., & Xu, G. (2019). Order spectrogram visualization for rolling bearing fault detection under speed variation conditions. *Mechanical Systems and Signal Processing*, *122*, 580–596.

Wigner, E. (1932, Jun). On the quantum correction for thermodynamic equilibrium. *Phys. Rev.*, *40*, 749–759. Retrieved from https://link.aps.org/doi/10.1103/PhysRev.40.74 doi: 10.1103/PhysRev.40.749

Williams, W. J. (1996). Reduced interference distributions: biological applications and interpretations. *Proceedings of the IEEE*, *84*(9), 1264–1280.

Williams, W. J., Brown, M. L., & Hero III, A. O. (1991). Uncertainty, information, and time-frequency distributions. In *Advanced signal processing algorithms, architectures, and implementations ii* (Vol. 1566, pp. 144–156).

Yardibi, T., Li, J., Stoica, P., Xue, M., & Baggeroer, A. B. (2010). Source localization and sensing: A nonparametric iterative adaptive approach based on weighted

least squares. *IEEE Transactions on Aerospace and Electronic Systems*, *46*(1), 425–443.

Zhang, R., & Castagna, J. (2011). Seismic sparse-layer reflectivity inversion using basis pursuit decomposition. *Geophysics*, *76*(6), R147–R158.

Zheng, G., & McFadden, P. (1999). A time-frequency distribution for analysis of signals with transient components and its application to vibration analysis.